JOURNAL OF THERMOPHYSICS AND HEAT TRANSFER
Vol. 10, No. 2, April–June 1996

Natural Convection over Rotating Cylindrical Heat Source in an Enclosure

N. K. Ghaddar*
American University of Beirut, Beirut, Lebanon

Mixed convection heat transfer induced by the mutual interaction between natural convection and a rotating cylindrical heat source in rectangular enclosures is investigated for different geometric settings of the heat source. The governing conservation equations of mass momentum and energy are solved numerically using the spectral element method. The numerical results are validated against experimental heat transfer correlations available on the natural convection of stationary heated bodies in enclosures. Heat transfer rates due to the heated cylinder rotation are found to depend on the location of the cylinder with respect to the enclosure bottom wall and on the enclosure size. When only natural convection is present, a decrease in the mean Nusselt number is observed as the cylinder is moved upward and as the enclosure AR is reduced. Rotation of the heat source decreases the mean Nusselt number of the cylinder by 10–20% at low Ra/Re_ω^2 as compared to the pure natural convection case when the source is stationary. Enhancement of heat transfer is present only for values of Ra/Re_ω^2 greater than 10. In all geometric configurations the maximum temperature on the cylinder surface is reduced by 10–25%, depending on the rotational speed and position of the heat source, and the Rayleigh number of the flow and the angular position of the maximum temperature is shifted from the top of the cylinder for the case of pure free convection to a new position in the direction of rotation.

Nomenclature

C = Courant number
d = cylinder diameter
g = gravitational acceleration
H = immersion depth from the enclosure top wall to the cylinder center
k = thermal conductivity of the fluid
L = enclosure height
Nu = local Nusselt number, Eq. (6)
Nu_m = mean Nusselt number on the cylinder
P = dimensionless pressure, Eq. (1)
Pr = Prandtl number, ν/α
p = pressure
q_w = uniform heat flux at the cylinder wall
Ra = Rayleigh number, Eq. (1)
Re_ω = rotational Reynolds number, $\omega r_0^2/2\nu$
r_0 = cylinder radius
T = temperature
t = dimensionless time
U = dimensionless velocity component in x direction
V = dimensionless velocity component in y direction
W = enclosure width
(x, y) = Cartesian coordinates
α = thermal diffusivity
β = thermal expansion coefficient
ΔT_c = $T_c - T_0$, where T_c is the temperature on cylinder surface and T_0 is the enclosure wall temperature
$\Delta\phi$ = angular shift of the maximum temperature position of the rotating source from that of fixed source
θ = dimensionless temperature, Eq. (1)
$\theta_{\max}$ = maximum dimensionless temperature on the cylinder surface
μ = fluid viscosity
ν = kinematic viscosity of the fluid
ρ_0 = density of the fluid
ϕ = angle measured clockwise from the negative x axis
ω = angular velocity of the cylinder

Subscripts
c = cylinder surface values
n = normal component
s = tangential component

Received May 1, 1995; revision received Aug. 26, 1995; accepted for publication Aug. 27, 1995.

*Associate Professor, Department of Mechanical Engineering. Member AIAA.

Introduction

PASSIVE natural convection cooling plays a prominent role in thermal management and control of cooling of heat sources in enclosures. A numerous number of investigations considered free convection in enclosures due to its extensive applications in nuclear safety design, electronic equipment cooling, crystal growth, and solar energy systems.[1,2] Chu et al.[3] studied free convection heat transfer from a discrete heat source in a two-dimensional enclosure. The local and average heat transfer were found to be strongly dependent on heater location and Grashof number. The numerical predictions of Chu et al. were later verified experimentally by Turner and Flack.[4] Methods for the enhancement of natural convection heat transfer in enclosures have also been considered. Gershuni and Zhukhoritsk,[5] Forbes et al.,[6] Biringen and Danabasoglu,[7] and Fu and Shieh[8] investigated thermal convection in an enclosure induced simultaneously by gravity and vibration and found that the heat transfer increased. Fu et al.[9] investigated numerically the enhancement of natural convection in a square enclosure with one heated vertical wall and in the presence of an insulated rotating circular cylinder. The contribution of the rotating cylinder natural convection heat transfer was found to depend on the rotation direction and was only substantial when Gr/Re_ω^2 was larger than 100. Applications for mixed convection in enclosures may be extended to rotary machine design, transpiration cooling, and rotary machines placed in confined regions such as silencers. Earlier work of Ghaddar and Thiele[10] on free convection over a cylindrical heat source in an enclosure found that rotation of the source reduced the maximum

surface temperature, but marginally affected the mean rates of heat transfer from the source.

The present study employs the spectral element method[11] to investigate numerically the effect of rotation on natural convection flow over a heat source placed in a rectangular isothermal enclosure. The study supplements the results of the earlier work and includes the effect of the heat source location, cavity aspect ratio, and extends the ranges of rotational speeds beyond those studied previously.

Physical Model

The proposed physical model for the study is sketched in Fig. 1. A rotating cylinder of $d = 2r_0$ is placed in a two-dimensional enclosure of L' and W'. The cylinder is located at a distance H' from the top wall of the enclosure and at a distance $W'/2$ from the side walls. All lengths are nondimensionalized with respect to d, such that $H = H'/d$, $L = L'/d$, and $W = W'/d$. The nonrotating x-y coordinate system is attached to the center of the cylinder. The cylinder is rotating at a constant ω normal to the xy plane in the clockwise direction. A constant q_w is applied at the cylinder surface, while the enclosure walls are assumed isothermal. The flow is assumed laminar with constant fluid properties, except for the induced density variations in the body force term.

The governing equations are nondimensionalized using the following definition of dimensionless variables:

$$X = x/d \qquad Y = y/d$$

$$U = u/\omega r_0 \qquad V = v/\omega r_0$$

$$P = (p + \rho_0 g y)/(\rho_0 \omega^2 r_0^2) \tag{1}$$

$$Re_\omega = \omega d^2/2\nu \qquad \theta = (T - T_0)/(q_w d/k)$$

$$Pr = \nu/\alpha \qquad Ra = g\beta d3(q_w d/k)/(\mu\alpha)$$

With the stated assumptions and the Boussinesq approximation, the dimensionless governing transport equations of mass momentum and energy are, respectively,

$$\frac{\partial U}{\partial X} + \frac{\partial V}{\partial Y} = 0 \tag{2}$$

$$\frac{\partial U}{\partial t} + U\frac{\partial U}{\partial X} + V\frac{\partial U}{\partial Y} = -\frac{\partial P}{\partial X} + \frac{1}{Re_\omega}\left(\frac{\partial^2 U}{\partial X^2} + \frac{\partial^2 U}{\partial Y^2}\right) \tag{3a}$$

$$\frac{\partial V}{\partial t} + U\frac{\partial V}{\partial X} + V\frac{\partial V}{\partial Y} = -\frac{\partial P}{\partial Y} + \frac{1}{Re_\omega}\left(\frac{\partial^2 V}{\partial X^2} + \frac{\partial^2 V}{\partial Y^2}\right) + \frac{Ra}{Re_\omega^2 Pr}\theta \tag{3b}$$

$$\frac{\partial \theta}{\partial t} + U\frac{\partial \theta}{\partial X} + V\frac{\partial \theta}{\partial Y} = \frac{1}{Re_\omega Pr}\left(\frac{\partial^2 \theta}{\partial X^2} + \frac{\partial^2 \theta}{\partial Y^2}\right) \tag{4}$$

The associated flow boundary conditions are the no-slip condition on the enclosure walls and specified velocities on the cylinder surface given by

$$U = \cos[\tan^{-1}(Y/X)] \tag{5a}$$

$$V = \sin[\tan^{-1}(Y/X)] \tag{5b}$$

where X and Y are the coordinates of points on the cylinder surface. The cylinder rotation is taken in the clockwise direction. The thermal boundary conditions are $\theta = 0$ at the enclosure wall and $q_w = -k(\partial T/\partial n) = \text{const}$, i.e., $\partial\theta/\partial n = -q_w d/k$ on the cylinder boundary, with n being the outward

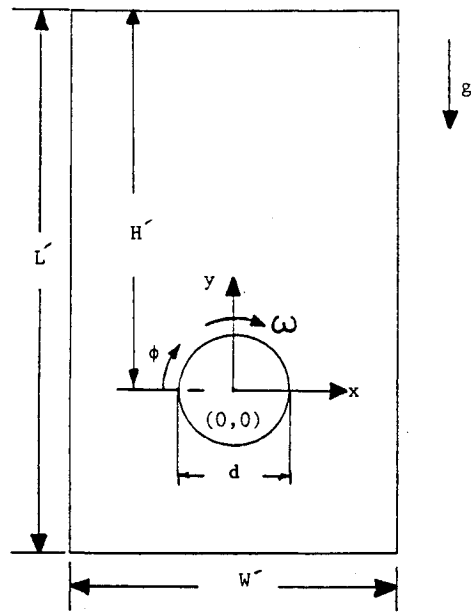

Fig. 1 Physical model geometry and the coordinate system of x and y attached to the center of the cylinder.

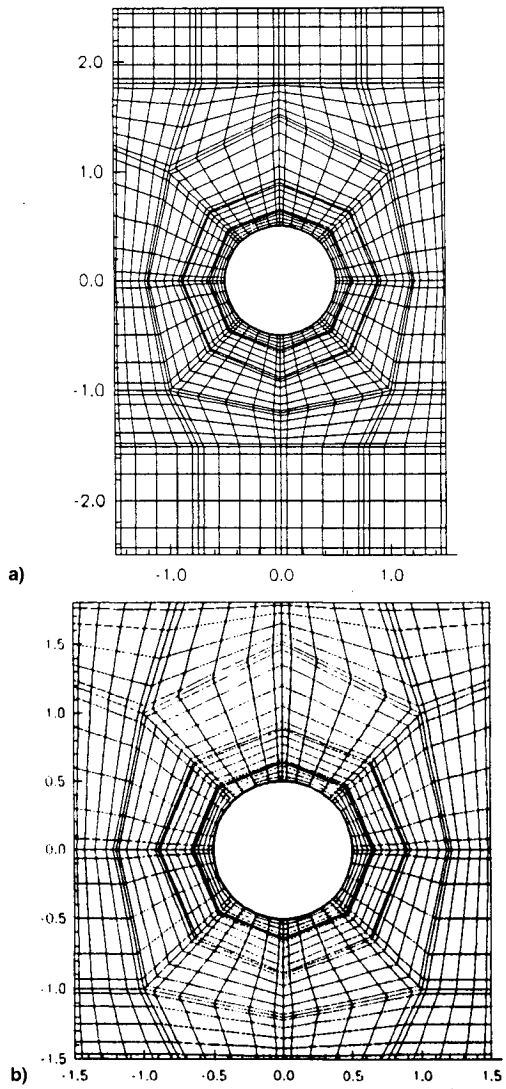

Fig. 2 Typical grid systems of two different geometries having a) 48 macroelements (G2) $L/W = 5/3$, $H/L = 0.5$ and b) 36 macroelements (G4) $L/W = 1.06$, $H/L = 0.53$, with $N \times N$ ($N = 7$) local spectral resolution.

normal on the cylinder surface. The physical quantity of primary interest is the local Nusselt number defined as

$$Nu(\phi) = (q_w/\Delta T_c)(d/k) = 1/\theta_c \quad (6)$$

where ΔT_c is the difference between the local temperature at the cylinder surface at any ϕ and T_0. The mean Nu_m is based on the average temperature of the cylinder. Another important correlating parameter is $Ra/(Pr^*Re_\omega^2)$, which appears in the buoyancy term of the momentum Eq. (3b). The geometric parameters of interest are the AR of the enclosure L/W and the immersion depth of the heat source from the top wall H/L. In the present work, four geometrical configurations are investigated corresponding to (G1) $L/W = 5/3$, $H/L = 0.3$, (G2) $L/W = 5/3$, $H/L = 0.5$, (G3) $L/W = 5/3$, $H/L = 0.7$, and (G4) $L/W = 1.06$, $H/L = 0.53$.

Numerical Solution

The previous coupled system of Eqs. (2–4) is solved numerically using the spectral element method.[12] The numerical approach of the spectral element code is that of direct simulation using initial value solvers. The method is a high-order, weighted residual technique that exploits both the common features and the competitive advantages of low-order finite element methods (generality and geometric flexibility) and the p-type spectral techniques (accuracy and rapid convergence).

The temporal discretization of the governing equations is performed using the multistep fractional scheme.[13] The convective nonlinear terms and the buoyancy term are marched in time using a third-order Adams–Bashforth scheme followed by a split pressure step that uncouples continuity and pressure equations by using an inviscid pressure boundary condition. The diffusion terms are treated implicitly in a final step using second-order Crank–Nicolson schemes. The method has temporal accuracy of order Δt for the velocities and a splitting error of $\Delta t^{1/2}$ for the pressure.

The spatial discretization of the computational domain is done by dividing the domain into general quadrangular macroelements. Within each element, the dependent and independent variables are presented in terms of high-order, tensor-product polynomial expansions with Chebyshev collocation points. Typical grid systems are shown in Figs. 2a and 2b for two of the different geometries investigated in this work, having 48 (G2) and 36 (G4) macroelements, respectively, with $N \times N$ ($N = 7$) local spectral resolution. Mixed variational and collocation operators are used to generate the discrete equations with interfacial continuity constraints imposed naturally via the variational statements. This approach results in a weak coupling between dependent variables in adjacent elements and relatively sparse matrices, making the method efficient and easy to implement. Spectral methods have proven to be very powerful for analyzing fluid flows and heat transfer because of their ability to represent accurately the thermofluid variables and resolve high local gradients with fewer grid points. The spectral element code had been used and tested for accurately simulating highly unsteady two-dimensional laminar flows with heat transfer.[13,14]

All of the calculations were done on similar grid systems shown in Fig. 2, but with higher spectral resolution ($N = 8$, 9) as Ra or Re_ω were increased. The total number of nodes in the computational domain varied from about 1800 to 3000 nodes. The computations were performed in double precision on a 486DX2-66-MHz personal computer using Watcom Fortran Compiler. The time step size Δt for the numerical solution is governed by the Courant number stability condition of $C = (\Delta t V_{max}/\Delta s) < 0.7$, where Δs is the minimum grid size in either the x or y direction. The minimum grid size was 0.65% of the cylinder diameter near the cylinder surface, whereas the dimensionless time step size was of the order 10^{-4}. The solutions were checked for convergence in both time-step and spatial degrees of freedom. The convergence criterion was set relative to the change in temperature. Convergence was achieved when the maximum change in temperature was less than 10^{-5}. A typical run takes about 40–60 h on the personal computer. Figure 3 shows a history plot of velocity and temperature for a given point in the domain at ($X = 1.0$, $Y = 0.5$) for (G2) at $Ra = 10^5$ and $Re = 100$. Also, an energy balance was performed for each simulation to verify that the total heat transferred through the enclosure isothermal walls was actually equal to the total heat input dissipated at the cylinder surface. At the steady-state conditions the error dif-

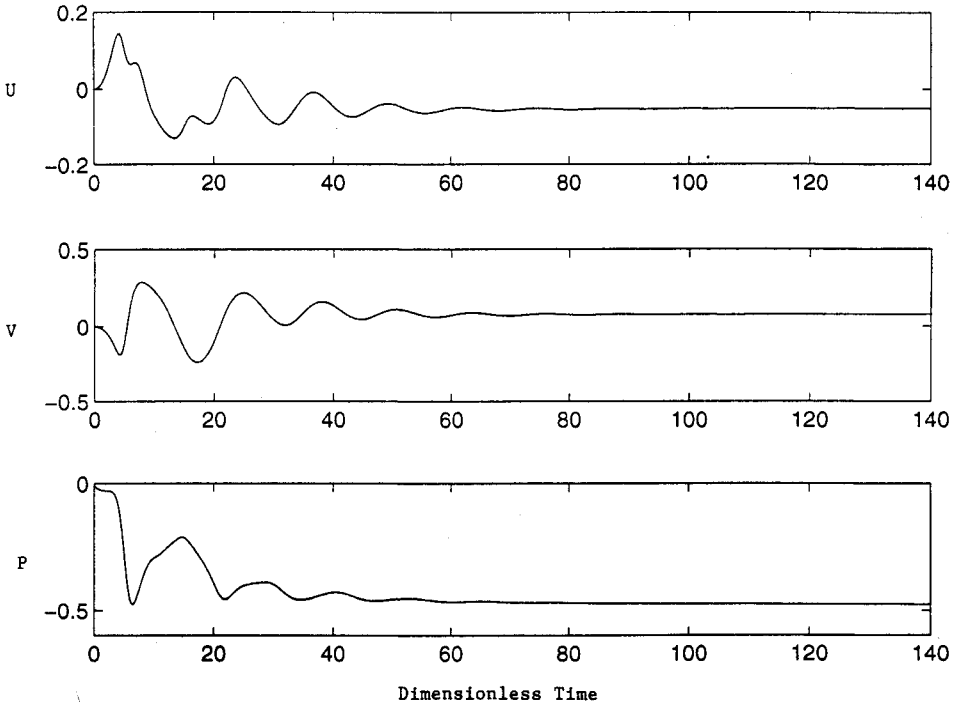

Fig. 3 History plot of V for a given point in the domain at ($X = 1$, $Y = 0.5$) for G2 at $Ra = 10^5$, $Re_\omega = 100$.

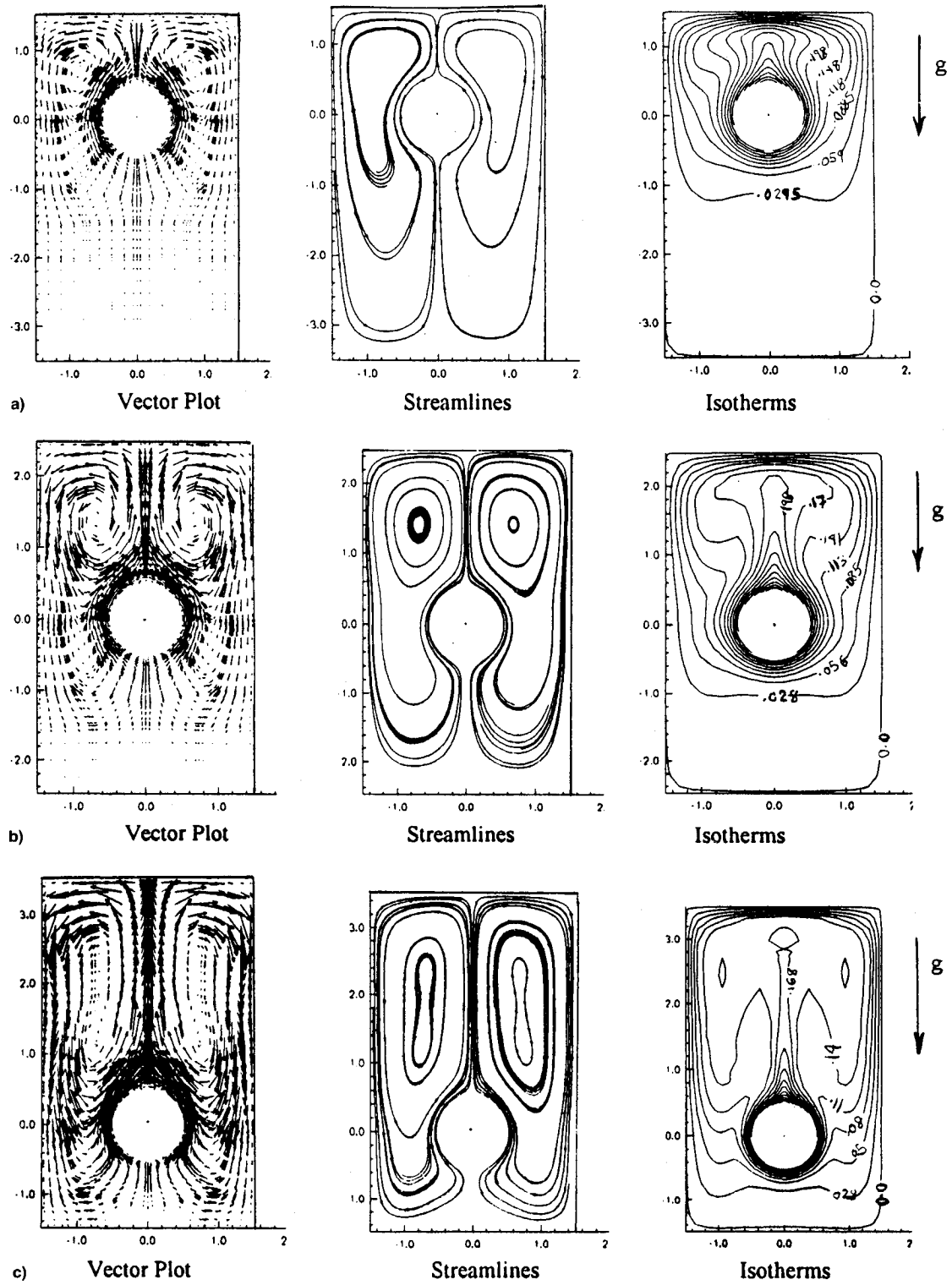

Fig. 4 Temperature and velocity fields of steady natural convection around the fixed heat source for three different immersion depths of H/L = a) 0.3, b) 0.5, and c) 0.7 in an enclosure of AR of $L/W = 5$, at $Ra = 10^4$.

ference in the balance was less than 0.01%. The validity of the computer simulation model was examined in earlier work of Ghaddar[15] and Ghaddar and Thiele[10] against published experimental correlations of Warrington and Powe[1] for the special case of pure natural convection between a heated body and its rectangular enclosure for air as a test fluid.

Results and Discussion

The numerical computations were carried out in four different geometrical configurations for a wide range of Rayleigh and Reynolds numbers that included limiting cases of conduction, zero rotation, and zero natural convection. The Prandtl number is set to one in all of the runs. In what follows the angular position on the cylinder starts at $\phi = 0$ on the negative x axis and increases on the clockwise direction as indicated in Fig. 1. Of special interest is the effect of the cylinder position in the enclosure on the mean Nusselt number, the maximum temperature of the heat source, and the power input to the fluid at various rotational speeds and flux conditions. Before the physical aspects of the flow and temperature fields

of the rotating source cases and the results of the parametric analysis are shown, the analysis is first presented for the case of natural convection between the heated fixed source and its rectangular enclosure.

Fixed Heat Source

The temperature and velocity fields of steady natural convection around the fixed heat source are presented in Figs. 4a–4c for three different immersion depths of $H/L = 0.3$, 0.5, and 0.7 in an enclosure of AR of $L/W = 5/3$, at the same Rayleigh number of 10^4. The motion is characterized by two identical counter-rotating cells induced by recirculations in which warm fluid rises with the plume above the cylinder and is cooled as it descends along the isothermal sides. As the heat source immersion depth is increased, a larger portion of the enclosure is affected by the buoyancy-driven flow and more of the cool wall is thermally active. The mean Nusselt number of the cylinder increases and the maximum temperature on its surface decreases as the immersion depth increases, as seen in Fig. 5, which shows the Nu_m and θ_{max} on the cylinder surface vs the immersion depth H/L at $Ra = 10^3$ and 10^4. The variation in Nusselt number is slight but noticeable, the difference being approximately 12% for the $H/L = 0.3$ and 0.7 extremes. The observed increase is due to the increased intensity of natural convection in the enclosure and increased interaction with the cooled isothermal wall, as has also been reported by Chadwick et al.[16] and Deschamps and Desrayaud.[17] The heat transfer profiles can be correlated using

$$Nu = BRa^A \tag{7}$$

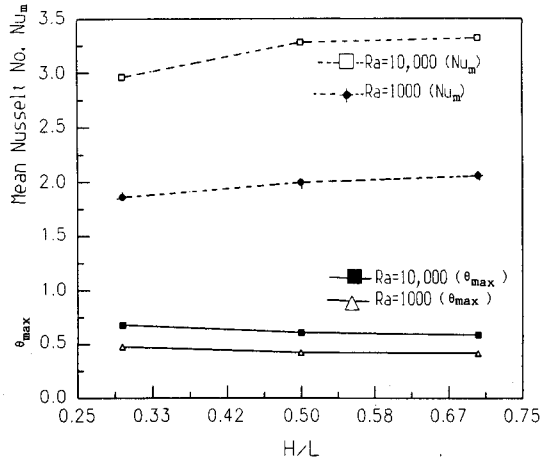

Fig. 5 Nu_m **and** θ_{max} **on the cylinder surface vs immersion depth** H/L **at** $Ra = 10^3$ **and** 10^4.

Table 1 Coefficients and exponents for correlation Eq. (7) for the fixed heater placed in an enclosure

Present work			Chadwick et al.[16] results		
H/L	B	A	H/L	B	A
0.3	0.4704	0.202	0.2	0.438	0.193
0.5	0.449	0.215	0.5	0.454	0.199
0.7	0.491	0.206	0.8	0.526	0.192

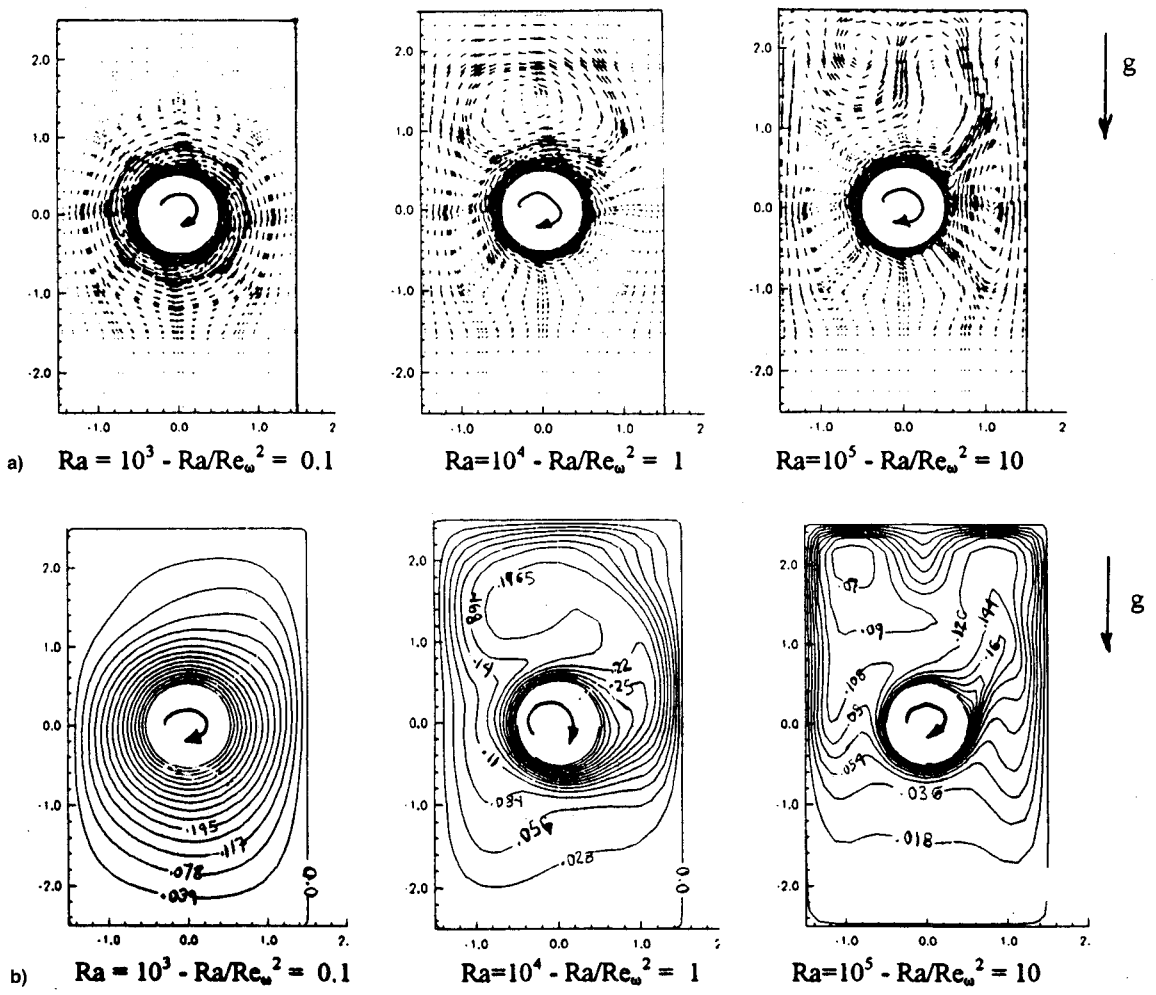

Fig. 6 Flow patterns of a) velocity vector plots and b) isotherms for values of 0.1, 1, and 10 of Ra/Re_ω^2 in enclosure G2 of the AR $L/W = 5/3$ and with the heat source immersion depth at $H/L = 0.5$.

The coefficients and exponents for various fixed heater locations are given in Table 1, including for comparison the coefficient and exponents found by Chadwick et al.[16] for a single vertical plate heater configuration placed in an isothermal enclosure of AR $L/W = 5$ and with enclosure length to heater size of 7.5. The coefficients and exponents were obtained from the least-squares regression fits over a range of Rayleigh numbers and with an average error of 3%. Our results for the cylindrical heater are consistent with those experimental and numerical correlations of Chadwick et al., presented in Table 1, even though the shape of the heater is not the same, but the mechanism of heat transfer, heater location, and range of Rayleigh numbers are consistent with our configurations. Previous studies have revealed that the maximum heat transfer occurs for a heater location near $H/L = 0.5$ for Rayleigh numbers significantly lower than those of this work.[3] Chu et al. also showed that the heater location corresponding to maximum heat transfer is Rayleigh-number-dependent, such that the maximum Nusselt number was found at higher H/L for increasing Rayleigh number. The slight difference in the slope of the predicted $Nu_m - Ra$ distribution for various locations of the heater is consistent with these findings. If one extrapolates the predictions of Nu_m to lower values of Ra, then the maximum Nu_m is indeed at $H/L = 0.5$ as predicted by Chu et al.[3]

Rotating Heat Source Configuration

To examine the effect of rotational speed of the cylinder on natural convection heat transfer of the enclosure, the rotational speed Re_ω is varied from 10 to 200 for Rayleigh numbers of 10^3, 10^4, and 10^5 with the Prandtl number set to 1 in four different geometrical configurations. Typical flow patterns illustrated by vectorplots and isotherms are presented in Figs. 6a and 6b for values of 0.1, 1, and 10 of Ra/Re_ω^2 in enclosure G2 of the AR $L/W = 5/3$ and with the heat source immersion depth at $H/L = 0.5$. Flow patterns and isotherms are also shown for the other three geometrical configurations G1, G3, and G4 by means of streamlines illustrated in Fig. 7a, and isotherms illustrated in Fig. 7b for the case of $Ra = 10^4$, $Re_\omega = 100$ corresponding to $Ra/Re_\omega^2 = 1$.

Figure 6a shows that the rotational motion dominates the mechanism of convection at the low Ra/Re_ω^2 and only the fluid near the cylinder has significant rotational motion while the rest of the region is almost stagnant. The circular isotherm patterns look very much like a conduction-dominant regime, except that the cylinder surface temperature attains a much lower temperature than the conduction case due to the centrifugal force in the fluid, as will be shown later. At higher $Ra/Re_\omega^2 \geq 1$, the rotation of the cylinder has caused the rising thermal plume to shift in the clockwise rotation direction as seen in Fig. 6b. The larger the value of Ra/Re_ω^2, the smaller the shift in the thermal plume centerline from the vertical y axis. The rising hot fluid diffuses the heat by conduction while reaching the far top enclosure walls. The region below the cylinder near the bottom wall remains mostly stagnant and cool. In the vicinity of the cylinder the fluid layer adjacent to the left side ($-90 < \phi < 90$) is moving upward, and hence, aiding the upward motion induced by natural convection. The

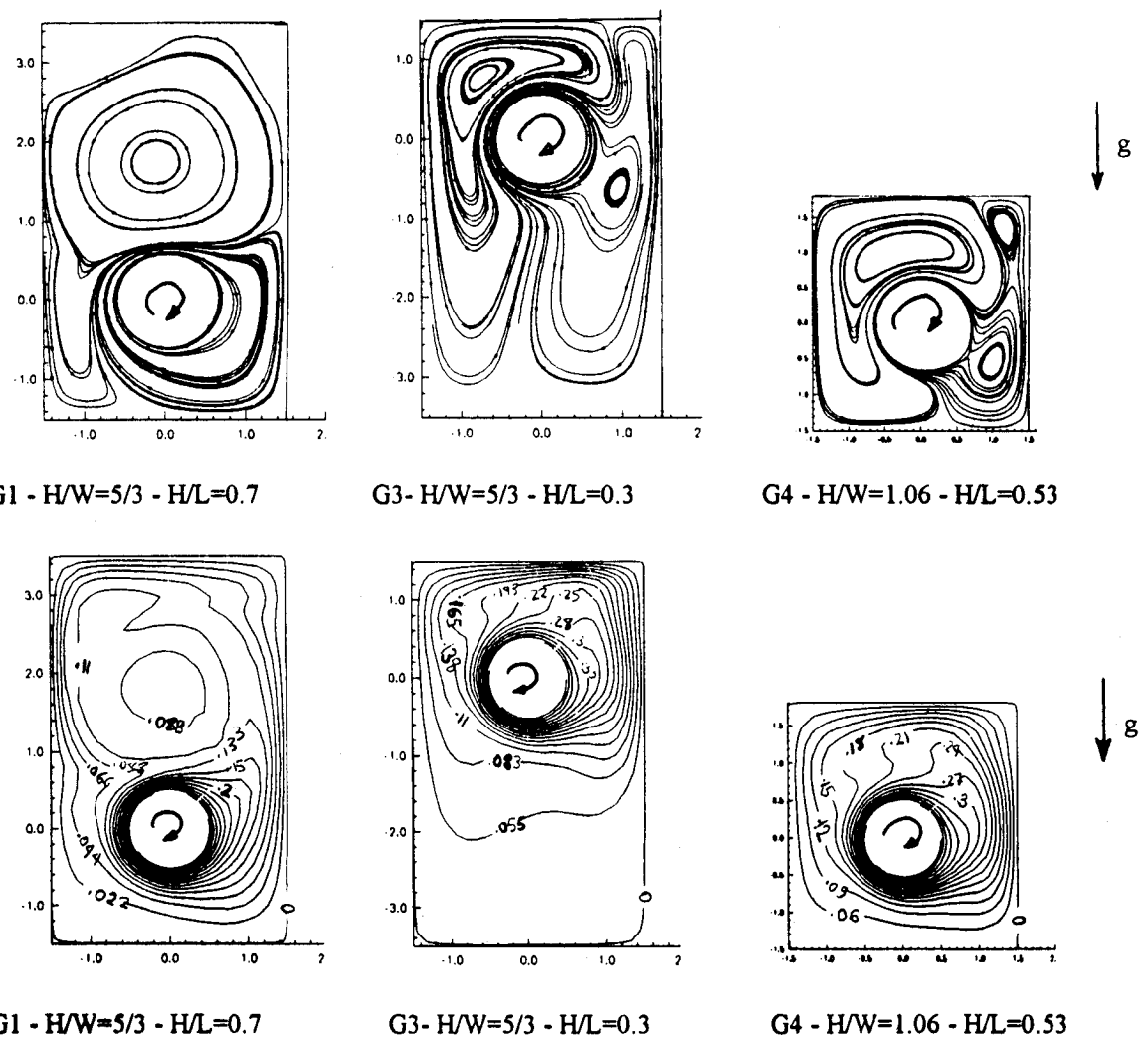

Fig. 7 Streamlines for the three geometrical configurations of a) G1, G3, and G4 at $Ra = 10^4$, $Re_\omega = 100$, and isotherms for the three geometrical configurations of b) G1, G3, and G4 at $Ra = 10^4$, $Re_\omega = 100$.

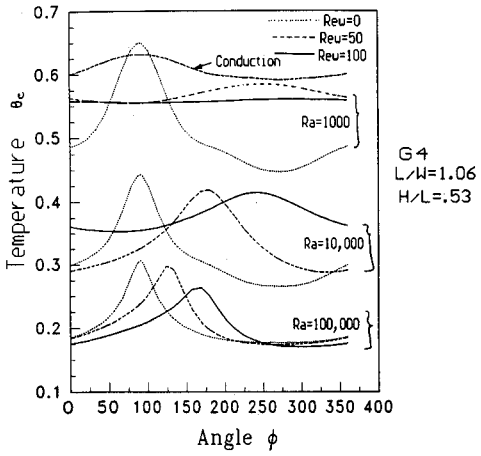

Fig. 8 Local temperature distribution around the cylinder at Ra = 10^3 and 10^4 for rotational speeds of 0, 50, and 100, also including the conduction solution.

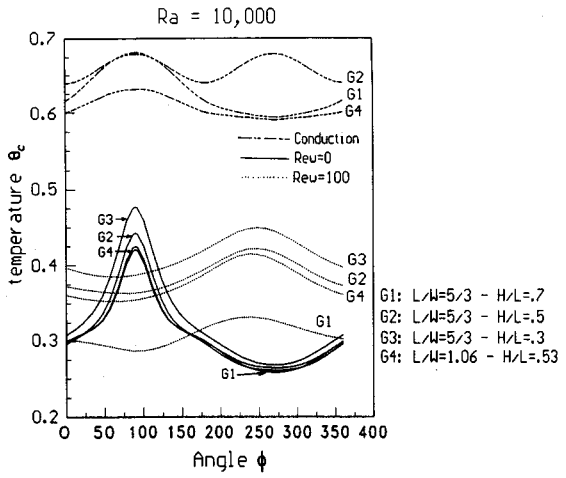

Fig. 9 Local temperature distributions at Ra = 10^4 at Re_ω = 0 and 100 for the four geometries of this study.

fast motion of the fluid on this side explains why the fluid on this side is cooler than the opposite side of $90 < \phi < 270$. On the right side of the cylinder, the fluid is moving downward in the opposite direction to the buoyed flow, slowing down the upward motion and bringing the hot boundary layer in contact with the cooler region below the cylinder. Comparatively, similar flow behaviors are observed when the depth of the heat source is changed or the AR of the enclosure is reduced (as seen comparing Figs. 6 and 7). Rotation of the cylinder disturbs only the convective flow around it in the enclosure while natural convection flow pattern is more dependent on the heat source location and enclosure AR.

The local temperature distribution on the cylinder is the one that is mostly affected by the rotation. Figure 8 shows local temperature distribution around the cylinder at Ra = 10^3, 10^4, and 10^5 for rotational speeds of 0, 50, and 100, including also the conduction solution in G4 of L/W = 1.06 and H/L = 0.53. At fixed Rayleigh number, the increase of rotation not only increases the shift of the maximum temperature from the geometrical position of ϕ = 90, but also decreases the value of θ_{max} and reduces the difference $\Delta\theta$ between the maximum and minimum temperatures. At high rotation rates (low Ra/Re_ω^2) the cylinder surface temperature is almost uniform. Figure 9 shows the local temperature distributions at Ra = 10^4 at Re_ω = 0 and 100 for the four geometries of this study. The angular shift in the maximum temperature position of the rotating cylinder case from the fixed case is not affected by the immersion depth change or the AR of the enclosure. The angular shift $\Delta\phi$ from its position when there is no rotation, $\Delta\phi = \phi_{\theta_{max}} - 90$ deg, is plotted in Fig. 10a as a function of $Ra/(Pr^* Re_\omega^2)$ using data of various immersion depths of the heat source. The decrease in the shift angle $\Delta\phi$ slows down as $Ra/(Pr^* Re_\omega^2)$ increases above 10. But the value of θ_{max} decreases with increased depth of the heat source, indicating that rotation of the source is more effective the closure it is to the enclosure bottom as seen from Fig. 10b, where θ_{max} is plotted as a function Ra/Re_ω^2 for various immersion depths of the heat source. The decrease in maximum temperature ranges from 10 to 23% and is larger at higher values of H/L.

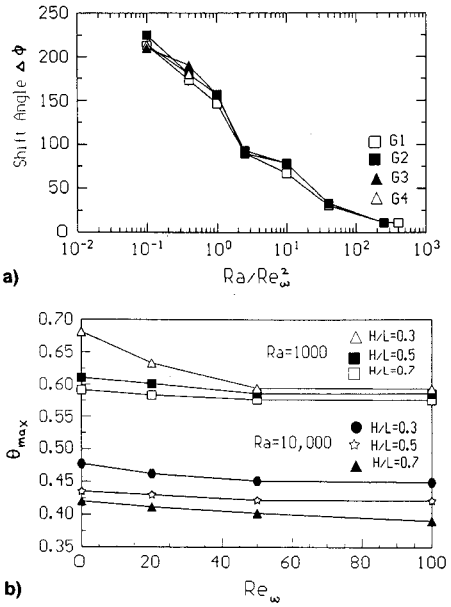

Fig. 10 a) $\Delta\phi$ of the maximum temperature from its position when there is no rotation $\Delta\phi = \phi_{\theta_{max}} - 90$ deg as a function of $Ra/(Pr^* Re_\omega^2)$ using data of various immersion depths at H/L = 0.3, 0.5, and 0.7 and b) maximum temperature θ_n as a function Ra/Re_ω^2 for immersion depths of the heat source of 0.3, 0.5, and 0.7 in the enclosure of AR of 5/3.

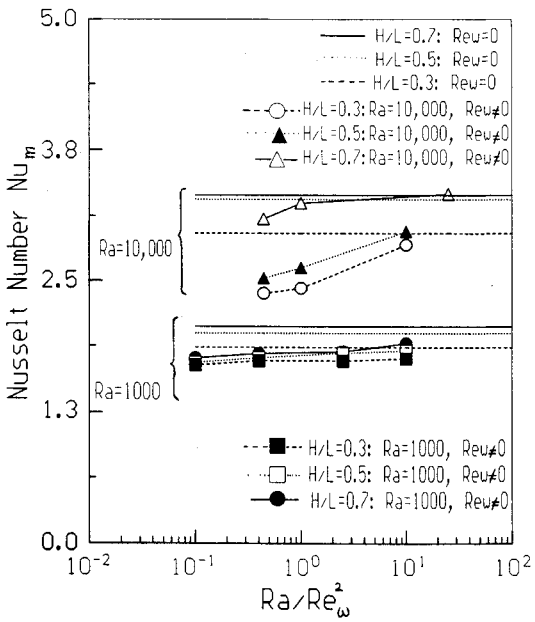

Fig. 11 Mean Nusselt number vs Ra/Re_ω^2 at Ra = 10^3, 10^4, and 10^5 for the enclosure of AR of 5/3 at different immersion depths of 0.3, 0.5, and 0.7, corresponding to geometries G1, G2, and G3. On the same plot the mean Nusselt number at zero rotation for each geometry and Rayleigh number is indicated.

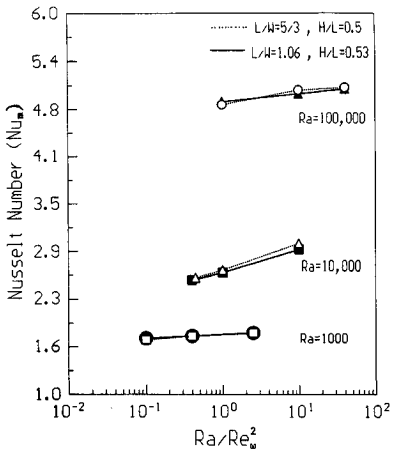

Fig. 12 Nu_m **vs** Ra/Re_ω^2 **at** $Ra = 10^3$, 10^4, **and** 10^5 **for the enclosures of ARs 1.67 and 1 with the immersion depth** $H/L \approx 0.5$.

Of interest here is relating the average heat transfer quantities on the cylinder surface to system parameters and comparing these average quantities with the limiting cases at zero rotation. In Fig. 11, the mean Nusselt number is plotted against Ra/Re_ω^2 at $Ra = 10^3$ and 10^4 for the enclosure of AR of 5/3 at different immersion depths of 0.3, 0.5, and 0.7 corresponding to geometries, G1, G2, and G3. On the same plot the mean Nusselt number at zero rotation for each geometry and Rayleigh number is indicated. At low values of Ra/Re_ω^2, rotation of the heat sources actually decreases the mean Nusselt number around the heat source as compared to the fixed cylinder of the same Rayleigh number. As Ra/Re_ω^2 increases, the mean Nusselt number increases and eventually slight enhancement of heat transfer is realized around the cylinder over a pure natural convection case for all of the geometrical configurations considered. The drop in Nusselt number reaches values up to 23% at $Ra/Re_\omega^2 = 0.44$ corresponding to $Ra = 10^4$, $Re_\omega = 150$, while in another case of $Ra/Re_\omega^2 = 250$ corresponding to $Ra = 10^5$, $Re_\omega = 20$, the Nusselt number increases by 5% for all of the immersion depths considered. It is obvious that increased rotation at any given Rayleigh number suppresses enhancement of heat transfer. The reason for this behavior is directly related to the reduction of the driving temperature difference for the upward motion as rotation ω is increased, since locally then the cylinder maximum surface temperature decreases and the temperature distribution is more uniform, added to the fact that the increase of motion on the left side of the cylinder due to rotation is counteracted by the opposition to motion on the right side. As Rayleigh increases for a given rotation rate, the upward velocities induced by natural convection exceed those induced by rotation of the cylinder and the rotation effect is confined to a very thin layer around the cylinder that causes a lower surface temperature, and thus, a higher mean Nusselt number than that found with zero rotation. These results are consistent with the early experimental work of Anderson and Saunders on free convection from an isolated rotating heated cylinder,[18] where they observed that the heat transfer was nearly constant at the free convection values until Ra/Re_ω^2 and Re_ω reached some critical values, after which the heat transfer rates increased.

To inspect the effect of AR of the enclosure on heat transport with the presence of rotation and natural convection, Nu_m is plotted in Fig. 12 against Ra/Re_ω^2 at $Ra = 10^3$, 10^4, and 10^5 for the enclosures of ARs 1.67 and 1.06 with the immersion depth $H/L \approx 0.5$. At a low Rayleigh number of 10^3, the mean Nusselt number is hardly dependent on the AR, while the maximum temperature is about 2% higher in the lower AR enclosure than that found in the higher AR. At higher Rayleigh numbers and $Ra/Re_\omega^2 > 1$, the higher AR has given slightly better values of the mean Nusselt number, indicating that rotation in this case is more effective in increasing heat transfer rates, due partly to the obstruction to upward motion by the isothermal top wall and the higher convective motion present in the whole enclosure, including the bottom region.

Conclusions

A spectral element method is used to investigate natural convection in isothermal enclosures due to the presence of a rotating cylindrical heat source.

Heat transfer rates due to the heated cylinder rotation are found to depend on the location of the cylinder with respect to the enclosure bottom wall and on the enclosure size. When only natural convection is present, the mean Nusselt number of the cylinder increases and the maximum temperature on its surface decreases as the immersion depth increases. Rotation of the heat sources at low values of Ra/Re_ω^2, actually decreases the mean Nusselt number around the heat source as compared to the fixed cylinder of the same Rayleigh number. As Ra/Re_ω^2 increases, the mean Nusselt number increases, and eventually, slight enhancement of heat transfer of no more than 5% is realized around the cylinder over pure natural convection case for all configurations considered here. The value of the maximum temperature decreases with increased depth of the heat source, indicating that rotation is more effective the closer the source is to the enclosure bottom.

Acknowledgment

The author would like to acknowledge the support of the University Research Board of the American University of Beirut enabling her to complete this work.

References

[1]Warrington, R. O., and Powe, R. E., "The Transfer of Heat by Natural Convection Between Bodies and Their Enclosures," *International Journal of Heat and Mass Transfer*, Vol. 28, No. 2, 1985, pp. 319–330.

[2]Keyhani, M., Parasad, V., Shen, R., and Wong, T. T., "Free Convection Heat Transfer from Discrete Heat Sources in a Vertical Cavity," *Natural and Mixed Convection in Electronic Equipment Cooling*, edited by R. A. Wirtz, American Society of Mechanical Engineers, New York, 1988, pp. 12–14.

[3]Chu, H. H. S., Churchill, S. W., and Patterson, C. V. S., "The Effects of Heater Size, Location, Aspect Ratio and Boundary Conditions on Two-Dimensional, Laminar Natural Convection in Rectangular Channels," *Journal of Heat Transfer*, Vol. 98, No. 1, 1976, pp. 194–201.

[4]Turner, B. L., and Flack, R. D., "The Experimental Measurement of Natural Convective Heat Transfer in Rectangular Enclosures with Concentrated Energy Sources," *Journal of Heat Transfer*, Vol. 102, No. 2, 1980, pp. 236–241.

[5]Gershuni, G. Z., and Zhukhovitsky, E. M., "Vibrational Thermal Convection in Zero Gravity," *Fluid Mechanics-Soviet Research*, Vol. 15, No. 1, 1986, pp. 63–84.

[6]Forbes, R. E., Carley, C. T., and Bell, C. J., "Vibration Effects on Convective Heat Transfer in Enclosures," *Journal of Heat Transfer*, Vol. 92, No. 2, 1970, pp. 429–438.

[7]Biringen, S., and Danabasoglu, G., "Computation of Convective Flow with Gravity Modulation in Rectangular Cavities," *Journal of Thermophysics and Heat Transfer*, Vol. 4, No. 2, 1990, pp. 357–365.

[8]Fu, W. S., and Shieh, W. J., "Study of Thermal Convection in an Enclosure Induced Simultaneously by Gravity and Vibration," *International Journal of Heat and Mass Transfer*, Vol. 35, No. 7, 1992, pp. 1695–1710.

[9]Fu, W. S., Cheng, C. S., and Shieh, W. J., "Enhancement of Natural Convection Heat Transfer of an Enclosure by a Rotating Circular Cylinder," *International Journal of Heat and Mass Transfer*, Vol. 37, No. 8, 1994, pp. 1885–1897.

[10]Ghaddar, N. K., and Thiele, F., "Natural Convection over a Rotating Cylindrical Heat Source in a Rectangular Enclosure," *Numerical Heat Transfer*, Pt. A, Vol. 26, 1994, pp. 701–717.

[11]Korzsak, K. Z., and Patera, A. T., "An Isoparametric Spectral

Element Method for Solution of the Navier-Stokes Equations in Complex Geometries," *Journal of Computational Physics*, Vol. 62, No. 2, 1986, pp. 361–379.

[12]Ghaddar, N. K., Karniadakis, G. E., and Patera, A. T., "A Conservative Isoparametric Spectral Element Method for Forced Convection: Application to Fully-Developed Flow in Periodic Geometries," *Numerical Heat Transfer*, Vol. 9, 1986, pp. 227–300.

[13]Orzsag, S. A., and Kells, L. C., "Transition to Turbulence in Plane Poiseulle and Plane Coutte Flows," *Journal of Fluid Mechanics*, Vol. 96, No. 1, 1980, pp. 159–178.

[14]Amon, C. H., and Mikic, B. B., "Flow Pattern and Heat Transfer Enhancement in Self-Sustained Oscillatory Flows," AIAA Paper 89-0428, Jan. 1989.

[15]Ghaddar, N. K., "Natural Convection Heat Transfer Between a Uniformly Heated Cylindrical Element and Its Rectangular Enclosure," *International Journal of Heat and Mass Transfer*, Vol. 35, No. 10, 1992, pp. 2327–2334.

[16]Chadwick, M. L., Webb, B. W., and Heaton, H. S., "Natural Convection from Two-Dimensional Discrete Heat Sources in a Rectangular Enclosure," *International Journal of Heat and Mass Transfer*, Vol. 34, No. 7, 1991, pp. 1679–1693.

[17]Deschamps, V., and Desrayaud, G., "Modeling a Horizontal Heat Flux Cylinder as a Line Source," *Journal of Thermophysics and Heat Transfer*, Vol. 8, No. 1, 1994, pp. 84–91.

[18]Anderson, J. T., and Saunders, O. A., "Convection from an Isolated Heated Horizontal Cylinder Rotating About Its Own Axis," *Proceedings of the Royal Society of London, Series A: Mathematical and Physical Sciences*, Vol. 218, 1953, pp. 555–562.